Phosphonylation Mechanisms of Sarin and Acetylcholinesterase: A Model DFT Study

Jing Wang,† Jiande Gu,*,†,‡ and Jerzy Leszczynski*,†

Computational Center for Molecular Structure and Interactions, Department of Chemistry, Jackson State University, Jackson, Mississippi 39217, and Drug Design & Discovery Center, State Key Laboratory of Drug Research, Shanghai Institute of Materia Medica, Shanghai Institutes for Biological Sciences, Chinese Academy of Sciences, Shanghai 201203, P. R. China

Received: January 18, 2006; In Final Form: February 20, 2006

Potential energy surfaces for the phosphonylation of sarin and acetylcholinesterase (AChE) have been theoretically studied at the B3LYP/6-311G(d,p) level of theory. The obtained results show that the phosphonylation process involves a two-step addition−elimination mechanism, with the first step (addition process) being the rate-determining step, while by comparison, the ensuing steps are very rapid. Stable trigonal bipyramidal intermediates are formed in the studied pathways. It is also revealed that the catalytic triad of acetylcholinesterase plays the catalytic role in the reaction by speeding up the phosphonylation process, as it does in the acylation reaction of ACh and AChE. The effect of aqueous solvation was accounted for via the polarizable continuum model. It is concluded that the enzymatic reaction here is influenced strongly by the solvent environment.

Introduction

Acetylcholinesterase (AChE)[1,2] (EC 3.1.1.7) is one of the fastest enzymes, especially for the reaction of a serine hydrolase. It is well-known that AChE has one important ligand binding site,[3−5] the acylation site, which lies at the bottom of the gorge, consisting of a catalytic triad (such as His440, Glu327, and Ser200 in *Tc*AChE). Organophosphorus acid anhydrides (OPs) are rapid, stoichiometric, and essentially irreversible inhibitors of serine hydrolases, which can act as "hemisubstrate" to trap the enzyme.[6−9] The results of studies of the reactions of the natural substrate (ACh) and the inhibitors with AChE have been widely reported.[10−21]

Sarin (*O*-isopropylmethylphosphonofluoridate) is one of the well-characterized OP type inhibitors. When sarin interacts with AChE, it blocks the active center of AChE by formation of a phosphonate ester bond to the active site on serine. The phosphonylation yields a considerably more stable and complicated sarin−serine adduct[22] and therefore inhibits the active enzyme action. The sarin−AChE adduct is proposed to undergo dealkylation by a carbonium ion mechanism, resulting in C−O bond cleavage of the phosphonate ester bond and the loss of enzyme activity of AChE (aging). The crystal structure of the aged phosphonylated AChE offers a structural explanation for the substrate selectivity of AChE and reveals the nerve agent reaction products (aging) at the atomic level.[8] The origins and diversity of the aging reaction in phosphonate adducts of serine hydrolase enzymes were explored by molecular mechanics and molecular dynamics combined with semiempirical calculations. The active site characteristics of AChE, trypsin, and chymotrypsin were compared by their diastereomeric adducts with soman, methylphosphonate monoester anions, and tetravalent carbonyl intermediates of the reactions of the natural substrates in each case.[9] The stereoselectivity of the phosphonylation reaction and the effects of adduct configuration on the aging process were examined by four stereomers of soman with two chiral centers for human AChE (HuAChE) and its selected active center mutants.[23] MALDI-TOF/MS analysis for various nerve agent phosphyl adducts with the active site of AChE was performed to resolve aging reaction pathways.[24] The molecular dynamics (MD) simulations using the CHARMM program were performed to assess the molecular origins of stereoselectivity of phosphonylation for the solution structures of the pentacoordinate and tetracoordinate P_SC_S and P_RC_S adducts of *Tc*AChE formed with soman.[25] Rate-limiting P−O fission was reported in the self-stimulated inactivation of acetylcholinesterase by 4-nitrophenyl 2-propyl methylphosphonate.[26]

Phosphonylation of the active-site serine of AChE reveals important phenomena in the AChE active properties that have attracted the attention of investigators for decades. However, the related mechanisms are still obscure. George et al. proposed that the biochemical mechanism of OP inactivation of AChE is a process initiated by precursory phosphorylation at the catalytic serine residue, and the phosphorylation of AChE by an OP is synchronous with the ejection of a leaving group to yield a stable, covalent phosphoserine ester bond.[27] It was assumed that serine phosphonylation probably occurs by an in-line displacement of the leaving group and with the intervention of a pentacoordinate transient whose lifetime depends on the electronic and steric nature of all substituents, not only the leaving group.[9,28−30] The reaction of chiral isomers of isoparathion methyl with solubilized rat brain cholinesterase (RBAChE) was studied to reveal the consequence of phosphorus stereochemistry upon the postinhibitory reaction kinetics of AChE poisoned by phosphorothiolates.[31] Mutant cholinesterases were supposed to possess enhanced capacity for reactivation of their phosphonylated conjugates.[32] Kovach and co-workers reported the temperature dependence of the solvent isotope effect for the catalytic recruitment in the inactivation of AChE by soman, of which the rate-limiting process is proposed with less contribution of a general-base-catalyzed heavy-atom reorganization and more contribution of an induced-fit conformational change.[33] Sol-

* Corresponding authors. E-mail: J. G. jiandegush@go.com; J. L. jerzy@ccmsi.us.
† Jackson State University.
‡ Chinese Academy of Sciences.

10.1021/jp060370v CCC: $33.50
Published on Web 03/18/2006

volysis of sarin and a VX [*O*-ethyl *S*-(2-diisopropylamino)ethyl methyl-phosphonothiolate] model compound were theoretically studied at the MP2/6-31+G(d)//mPW1K/MIDI! level, and the results support the initial formation of trigonal bipyramidal intermediates and demonstrate kinetic selectivity for nucleophilic attack on the face opposite the more apicophilic methoxide ligand.[34]

In the present study, the density functional theory has been applied to probe the mechanism of the phosphonylation reaction between sarin and the active site serine of AChE. To illustrate the catalytic power of AChE in the phosphonylation reaction, reaction pathways under two extreme circumstances have been studied. They model the situation with and without the effect of the catalytic triad of AChE, respectively. The effect of aqueous solvation was accounted for via the polarizable continuum model (PCM) at the same calculation level to evaluate the solvent influences on the studied reactions.

Methods

All of the studied models have been fully optimized by analytic gradient techniques. The density functional theory (DFT) with Becke's three-parameter (B3)[35] exchange functional along with the Lee−Yang−Parr (LYP)[36,37] nonlocal correlation functional (B3LYP) was applied in this study. The standard valence triple-ζ basis set, augmented with d-type polarization functions for heavy elements and p-type polarization functions for H, 6-311G(d,p),[38] was used. In the analysis of harmonic vibrational frequency, the force constants were determined analytically for all of the complexes. The stationary structures are found by ascertaining that all of the harmonic frequencies are real. The structures of the transition states were obtained by verifying that one of the harmonic frequencies is imaginary and also by carrying out the intrinsic reaction coordinate (IRC) analysis for the reaction pathways. Natural Population Atomic (NPA) charges were determined using the same theoretical level with the Natural Bond Order (NBO) analysis of Reed and Weinhold.[39−42] All DFT computations were performed by using the *Gaussian 03* package of programs.[43]

The atoms-in-molecules (AIM) theory of Bader[44,45] was applied to characterize the noncovalent interactions of the studied models. In this study, the AIM analysis is carried out by the AIM2000 package (version 2.0),[46] based on the wave functions obtained at the B3LYP/6-311G(d,p) level of theory. The polarizable continuum model self-consistent reaction field of Tomasi and co-workers with a dielectric constant $\epsilon = 78.39$ (water)[47] was applied for all gas-phase-optimized structures to evaluate the solvation effects on the reactions.

Results and Discussions

The role of the nerve agent sarin on the suppression of the enzyme activity of AChE is that it restrains the catalytic triad by irreversible phosphonylation on the serine residue of the triad. The predictions of this reaction using the reliable DFT theory are not feasible if one considers the whole system. However, this reaction could be studied for properly constituted model species. To explore the phosphonylation reaction mechanism between sarin and acetylcholinesterase and to reduce the computational cost, the isopropyl group of sarin was modeled by a methyl group, creating the sarin model (*O*-methyl methylphosphonofluridate). The simplest selection of the model to represent AChE is the serine residue because the phosphonylation reaction occurs at the active serine site of AChE. Even this serine residue can be further simplified to methanol CH_3OH since the serine in the phosphonylation reaction acts as nucleophilic agent through its hydroxyl group at the ω position. However, serine as a reactant is partly deprotonated. At the active site the serine residue is made more nucleophilic by transferring its proton to the imidazole nitrogen of the histidine residue in the catalytic triad. The resultant imidazolium ion is further stabilized by the polarizing effect of the carboxylate ion of the glutamic acid residue in the triad. While an analysis of the reaction between unprotonated serine and sarin is useful, it is not fully relevant to the catalytic effect of the AChE enzyme. It is more instructive to consider a reference reaction that involves the same reactants as the corresponding nonenzymatic reaction to define the mechanism. In addition, different models considered in this study allow investigating in detail a role of selected molecular fragments that might govern these reactions. Therefore, both the deprotonated CH_3O^- anion and neutral CH_3OH were considered in this study. The former describes the reaction when the proton of the hydroxyl group of serine has totally transferred to the histidine residue (the A Pathway), and the latter represents the opposite extreme situation that serine holds the proton when the phosphonylation reaction occurs (the B Pathway). Thus, the catalytic role of the anionic and neutral reactants in the inhibition reaction can be estimated through comparison of these two extreme conditions.

A Pathway. The structures of the reactants, the intermediates, and the products of the model system were located as the local minima on the potential energy surface (PES). The corresponding transition states were characterized by the existence of single imaginary vibrational frequencies as the saddle points on the corresponding PES. An intrinsic reaction coordinate (IRC) analysis confirmed the transition states to connect the corresponding minima. The structures of all intermediates and transition states in the A Pathway are shown in Figure 1, and the reaction coordinate is depicted in Figure 2. The energy properties of all related structures in the reaction are summarized in Table 1.

In this reaction pathway, anionic CH_3O^-, which is H-bonded to the sarin model in the reactant complex INTa1, attacks the phosphorus atom of sarin and forms an intermediate product, INTa2. Subsequently, the P−F bond in INTa2 breaks, and a fluorine anion is released to form the final product INTa3. This is a two-step addition−elimination reaction pathway.

When the separated reactants (sarin model and the unprotonated serine model CH_3O^-) are mixed together, tetrahedral intermediate INTa1 is formed, which is stabilized through a weak CH···O type hydrogen-bonding interaction between the oxygen of serine (O_1) and the hydrogen from the methyl group of sarin, with an atomic distance of 1.69 Å and a bond angle of 167.5°. The density of the bond critical point (BCP) is predicted to be 0.0526 au through AIM analysis. For INTa1, the atomic distance between P and O_1 is 3.69 Å, indicating no interaction between these two species. INTa1 lies 36.3 kcal/mol below the separated reactants, implying that INTa1 is easy to be formed and stabilized after the reactants meet.

The activation energy of the formation of the transition state in serine's nucleophilic attack (TSa1) is found to be 4.9 kcal/mol (5.5 kcal/mol after the zero point correction). The single imaginary frequency of TSa1 is 112i cm^{-1}. The vibrational mode corresponding to the imaginary frequency reveals the direct nucleophilic attack of oxygen (O_1) of the model serine on the phosphorus atom of sarin from the backside of the fluorine in a slightly nonlinear fashion (with the O_1-P-F angle of 161.8°). The atomic distance of $P-O_1$ is 2.70 Å, about 0.99 Å shorter than that in INTa1. Furthermore, the AIM analysis predicts the BCP density and the Laplacian of densities at the BCP of $P-O_1$ as 0.0229 and 0.0528 au, respectively, implying

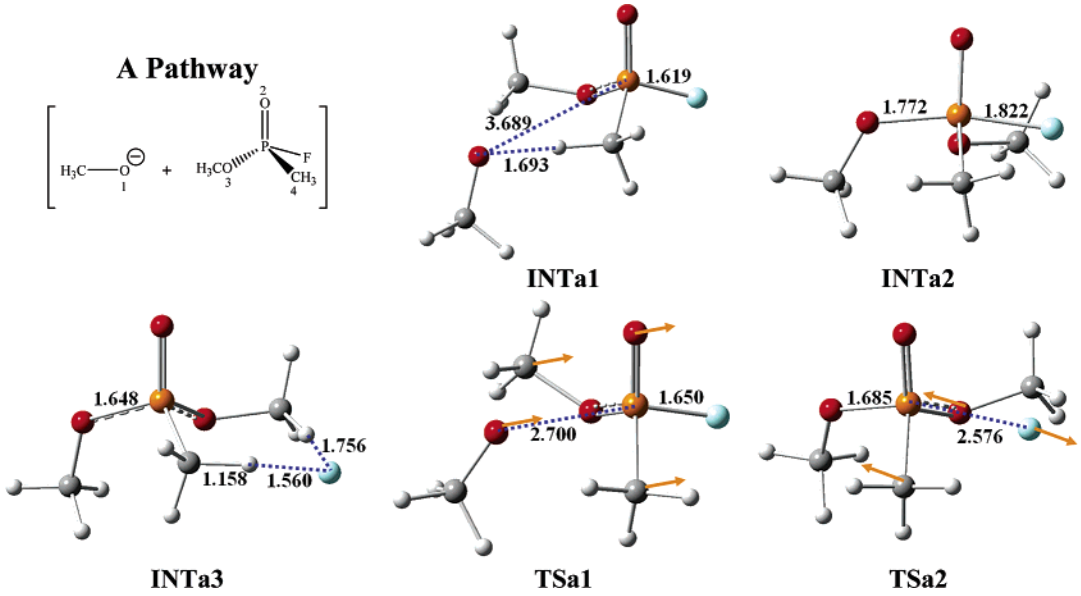

Figure 1. Optimized structures of all intermediates and transition states in the A Pathway. (Atomic distances in angstrom; INT represents intermediate, and TS represents transition state; F in aqua, P in orange, O in red, C in gray, and H in white balls; orange arrows illustrate the vibrational mode of the transition states.)

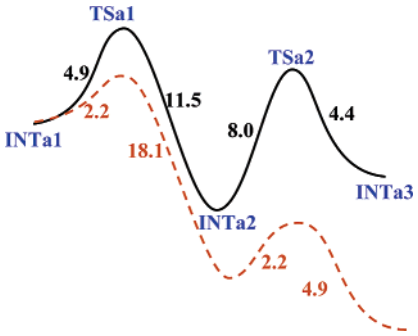

Figure 2. A Pathway of phosphonylation reaction between serine and sarin. (Pathway in gas phase is a black line, and the energy barrier values are in black; pathway from PCM models is an orange dotted line, and the energy barrier values are in orange. Energy unit in kcal/mol.)

the noncovalent interaction between P and O_1. The bond length of P−F increases (1.62 Å in INTa1) to 1.65 Å in TSa1, initializng the weakening of the P−F bond at the same time. The orientations of the methyl and methoxy groups of sarin remain almost the same as those in INTa1. The Gibbs free energy of activation between INTa1 and TSa1 is expected to be 7.0 kcal/mol (at 25° C, 1 atm pressure). The equilibrium constant of this step is therefore calculated to be 7.3×10^{-6}. The Natural Population Atomic (NPA) charges determined at the same theoretical level reveal that the negative charge distributed on the attacking oxygen of serine O_1 is −0.94 au, indicating the strong nucleophilic property of the unprotonated serine.

The most noticeable conclusion for the A Pathway is that, instead of being the pentacoordinated phosphorus transient species,[9,30] the trigonal bipyramidal structure of the pentacoordinated phosphorus compound (INTa2) forms a relatively stable local minimum in this reaction pathway. The methoxy group of sarin in INTa2 is rotated toward the fluorine atom. The P−O_1 distance is shortened to 1.77 Å. Although the P−F bond length is stretched to 1.82 Å, suggesting that this bond is weakened in the predicted intermediate, the bonding interaction still exists between phosphorus and fluorine. The NBO analysis shows that the net occupation of the P−F bonding orbital is 1.74. The energy of the transition state (TSa1) connecting INTa2 and the reactant (H-bonded CH_3O^- and sarin complex, INTa1) is 11.5 kcal/mol higher than that of INTa2. On the other hand, the energy barrier for P−F bond breaking in INTa2 amounts to 8.0 kcal/mol. Moreover, compared with the separated products (sarin−serine complex and F^-), the P−F bond dissociation energy for INTa2 is estimated to be more than 57 kcal/mol. INTa2 is located as the lowest energy structure on the potential energy surface of the A Pathway. Therefore, this pentacoordinated phosphorus compound is a stable intermediate product in the phosphonylation of serine by sarin, and one should be able to detect it by experimental techniques. Such an experiment could provide a final verification of the proposed mechanisms.

The transition state for the removal of fluorine from phosphorus (TSa2) could be reached from INTa2 by overcoming an energy barrier of approximately 8 kcal/mol (7.5 kcal/mol after the zero point correction). The geometry of TSa2 displays a nearly trigonal bipyramidal structure, with a dihedral O_2CO_3P angle and a bond O_1−P−F angle of −16.8° and 165.2°, respectively. The P−F bond is broken in TSa2, with an atomic distance of 2.58 Å. The P−O_1 bond is strengthened as its distance is shortened to 1.69 Å. The imaginary frequency of TSa2 is estimated as 147i cm^{-1}, and the vibrational mode indicates that fluorine is clipped by the methyl and methoxy groups from both sides and gets ready to leave the sarin−serine adduct. The NPA result shows that the negative charge distributed around the fluorine atom increases to −0.82 au (−0.68 au in TSa2). The HOMO orbital of TSa2, as shown in Figure 5, illustrates that the p-orbitals of the two carbons from the methyl and methoxy groups are both involved in the interaction with fluorine and assist the fluorine atom departure. The Gibbs free energy difference for this step is computed to be 7.3 kcal/ mol (at 25 °C, 1 atm pressure), only a bit higher than that of the first step. The equilibrium constant of this step is calculated to be 4.4×10^{-6}.

The INTa3 intermediate is only 4.4 kcal/mol lower in energy than TSa2, where the fluorine interacts with the hydrogen of the methyl group by a strong hydrogen bond (with a bond length of 1.56 Å and a bond angle of 167.0°). The atomic distance of phosphorus and fluorine is predicted to be 3.62 Å. INTa3 lies

TABLE 1: Energy Properties of the Reaction Structures at the B3LYP/6-311G(d,p) Level (kcal/mol)

structures	ΔE	ΔE_{ZPE}	$\Delta G0$	ΔE_{PCM}
		A Pathway		
INTa1[a]	0.0	0.0	0.0	0.0
	(−786.84726)	(−786.72211)	(−786.75975)	(−786.93016)
TSa1	4.9	5.5	7.0	2.2
INTa2	−6.6	−4.5	−3.2	−15.9
TSa2	1.3	3.0	4.1	−13.7
INTa3	−3.1	−1.7	−1.1	−18.6
		B Pathway		
INTb1[b]	0.0	0.0	0.0	0.0
	(−787.44341)	(−787.30173)	(−787.34142)	(−787.45002)
TSb1	31.0	28.5	30.4	30.1
INTb2	12.6	13.6	16.1	9.2
TSb2	23.0	22.8	25.4	17.4
INTb3	14.4	15.2	17.6	10.6
TSb3	23.1	22.3	24.4	20.6
INTb4	1.6	1.1	2.9	-2.5

[a] The energy differences are calculated based on the energy value of INTa1 (listed in parentheses with unit of au). [b] The energy differences are calculated based on the energy value of INTb1 (listed in parentheses with unit of au).

53.5 kcal/mol below the separated products, indicating its stabilization after the fluorine-elimination reaction.

It can be concluded that the reaction along the A Pathway could proceed easily. The first step reaction, which is the neucleophilic attack of serine on sarin, is supposed to be the rate-determining step.

The above discussion is based on the results of gas-phase calculations. To evaluate the solvent effects on this reaction, the PCM model (water solvent) was applied for reactants, intermediates, transition states, and products of the A Pathway. The potential energy surface of the A Pathway with the consideration of PCM effects is revealed with the orange dotted line in Figure 2. It shows that the solvent-mediated pathway is similar to the gas-phase pathway. However, the activation energy barrier for the rate-determining step is only half of that in the gas phase (2.2 kcal/mol). The transition state TSa1 releases more than 6 kcal/mol compared to the gas phase to reach intermediate INTa2. Moreover, the second energy barrier for the removal of fluorine is almost 6 kcal/mol lower than that in the gas phase, implying that the reaction occurs more easily under solvent conditions. Our results suggest that the solvent helps to speed up the phosphonylation reaction between sarin and AChE, and the entire reaction becomes almost barrierless in the solvent.

B Pathway. All relative structures of the intermediates and transition states for the B Pathway are depicted in Figure 3. The reaction pathway is presented in Figure 4. Similar to the A Pathway, the B Pathway also reveals a two-step addition−elimination reaction mechanism.

In the B Pathway, the neutral protonated serine model (methanol) acts as the nucleophile binding to the phosphorus of sarin while its proton simultaneously transfers to the oxygen of the phosphono group of sarin. In the following reaction, this transferred proton helps to break the P−F bond of the sarin−serine complex and the departure of fluorine as fluorine hydride (HF).

When the separated reactants (methanol and the sarin model) are mixed, the protonated serine first forms an intermediate complex (INTb1) with sarin through a hydrogen bond between its H_1 proton and the O_2 oxygen from sarin. The bond length and bond angle of the $O_1H_1\cdots O_2$ H−bond are predicted to be 1.94 Å and 145.2°, and the density of the BCP and the Laplacian of the density at the BCP are calculated by AIM analysis to be 0.0257 and 0.0958 au, respectively. INTb1 lies 9.1 kcal/mol below the separated reactants. The bond length of P−F in INTb1 is calculated to be 1.60 Å, while the distance between the oxygen of serine O_1 and the phosphorus atom is estimated to be 3.28 Å. NPA analysis shows that the negative charge distributed on O_1 is −0.77 au. The H_1 proton on serine is expected to transfer to the oxygen of the phosphono group of sarin when the phosphonylation reaction occurs.

Transition state TSb1 is found to be characterized by a pentacoordinated phosphorus compound with a tetrahedral structure. It lies 31.0 kcal/mol above the intermediate INTb1, indicating a 26 kcal/mol higher energy barrier for the first addition reaction step than that in the A Pathway. The single imaginary frequency of TSb1 is predicted to be 1298i cm^{-1}, corresponding to the vibrational mode of the proton (H_1) transferring from O_1 of serine to O_2 of sarin and the simultaneous necleophilic attack of the serine O_1 oxygen to the phosphorus. The atomic distances of H_1O_1 and H_1O_2 are estimated to be 1.26 and 1.19 Å, while the BCP densities are predicted to be 0.1524 and 0.1844 au, respectively, suggesting two strong hydrogen-bonding interactions of H_1 with O_1 and O_2. The NPA result displays a −0.84 au negative charge around O_1 of serine, suggesting that the possibility for a nucleophilic attack of serine is weaker than that described by TSa1 of the A Pathway. The atomic distance of P−O_1 is evaluated to be 2.05 Å (0.65 Å shorter than that in TSa1). Due to the existence of the H_1 proton, the p-orbital of the O_2 oxygen takes part in the bonding interaction between serine and sarin (as shown in the HOMO of TSb1 in Figure 5.). The P−F bond is elongated to 1.64 Å (1.60 Å in INTb1). The atomic angle of O−P−F in TSb1 is predicted to be 173.7°, indicating the linear necleophilic attacking reaction step. The Gibbs free energy of activation is predicted to be 30.4 kcal/mol (at 25 °C, 1 atm pressure), and the equilibrium constant of this step is calculated to be 5.1×10^{-23}, which shows about 17-fold of rate reduction compared to the corresponding step in the A Pathway.

The trigonal bipyramidal intermediate INTb2 lies 18.4 kcal/mol below TSb1. However, INTb2 is 12.6 kcal/mol higher than the separated reactants. The bond distance of P−O_1 is shortened to 1.71 Å (0.34 Å shorter than that in TSb1). Meanwhile, the P−F bond is predicted to be 1.69 Å, which is slightly longer (0.05 Å longer) than that in TSb1.

The H_1 proton, which was transferred from serine to sarin in the first step, was found to rotate around the P−O bond to the orientation of the fluorine atom in order to assist the departure of fluorine. The transition state TSb2 is characterized by being 10.4 kcal/mol above the intermediate INTb2. Its imaginary frequency is calculated to be 514i cm^{-1}, and the corresponding

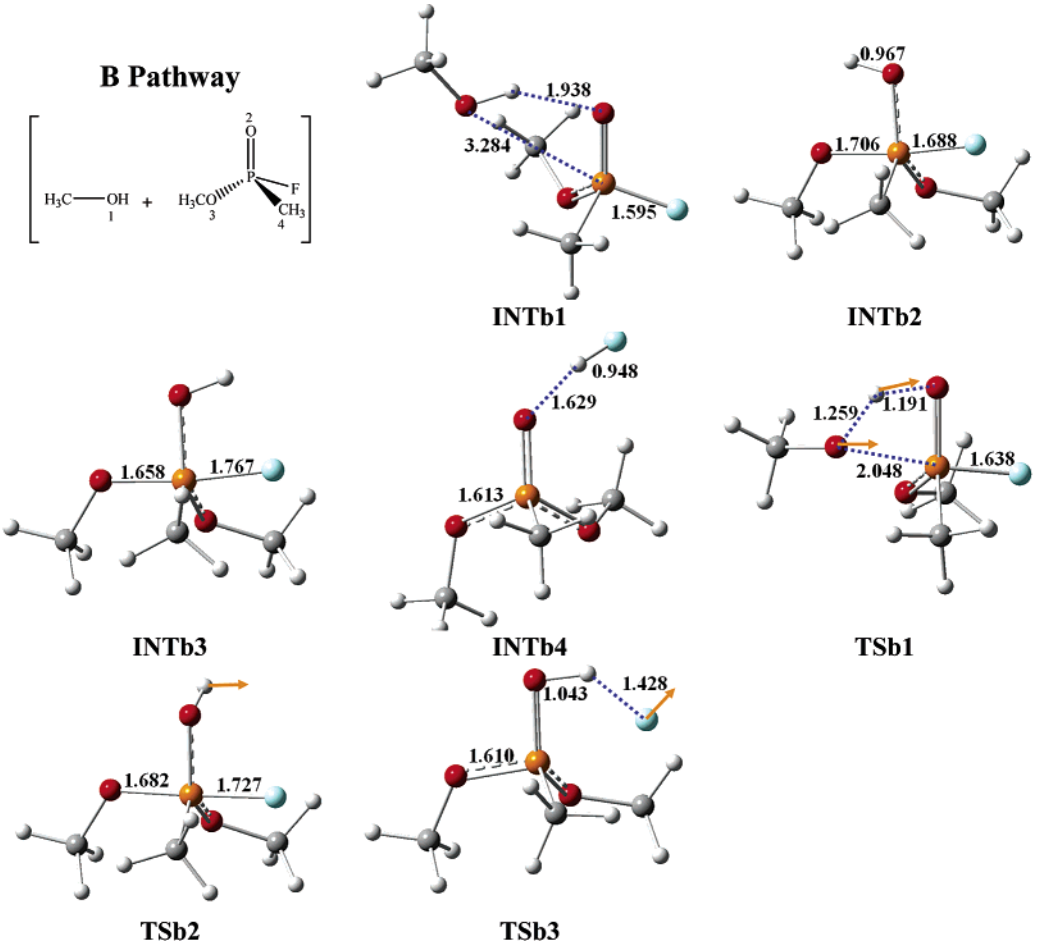

Figure 3. Optimized structures of all intermediates and transition states in the B Pathway. (Atomic distances in angstrom; INT represents intermediate, and TS represents transition state; F in aqua, P in orange, O in red, C in gray, and H in white balls; orange arrows illustrate the vibrational mode of the transition states.)

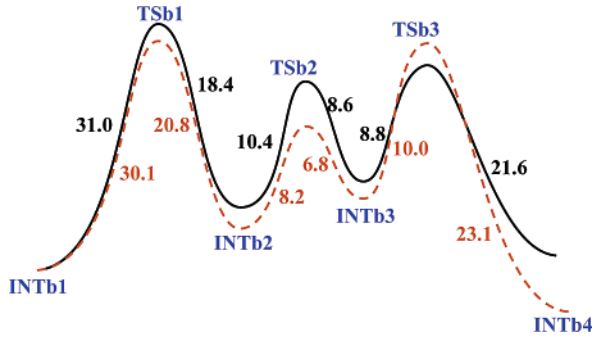

Figure 4. B Pathway of phosphonylation reaction between serine and sarin. (Pathway in gas phase is a black line, and the energy barrier values are in black; pathway from PCM models is an orange dotted line, and the energy barrier values are in orange. Energy unit in kcal/mol.)

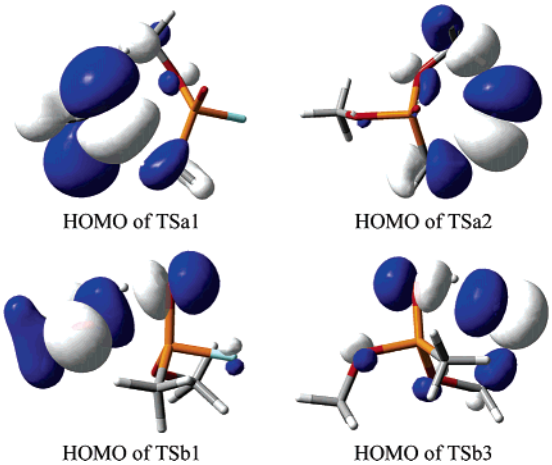

Figure 5. HOMO of the transition states for the A Pathway and the B Pathway.

vibrational mode indicates the rotation of H_1 from the side of O_1 to the opposite side where F is located. TSb2 also adopts the trigonal bipyramidal structure as INTb2. Moreover, the P−F bond is stretched to 1.73 Å, and O_1, P, and F are still kept in-line (with an atomic angle of 176.8°). The difference of Gibbs free energy between INTb2 and TSb2 is evaluated to be 9.3 kcal/mol, while the equilibrium constant is calculated to be 1.5×10^{-7}. After the proton is reorientated toward the fluorine side, the second pentacoordinate trigonal bipyramidal intermediate INTb3 is found to lie 8.6 kcal/mol below TSb2. INTb3 is characterized by the P−F bond stretched to 1.77 Å, and P−O_1 is strengthened to 1.66 Å.

The transition state TSb3 characterizes the fluorine departure process for the elimination step. Fluorine interacts with the H_1 proton by a strong hydrogen bond; the H_1−F bond distance is 1.43 Å, and the density of BCP is 0.0864 au. Meanwhile the bond distance between phosphorus and fluorine is stretched from 1.77 Å in TSb3 to 2.29 Å in TSb3, suggesting significant weakening of the P−F interaction. The results of NBO analysis indicate that the P−F bond is completely broken already in TSb3. The imaginary frequency is predicted to be 321i cm^{-1}, which corresponds to the vibrational mode of the leaving

fluorine atom which simultaneously interacts with the H_1 proton by the hydrogen-bonding interaction. While fluorine leaves the sarin−serine adduct, it no longer stays in-line with O_1 and P (the atomic angle of O_1PF is estimated to be 168.5°). TSb3 is characterized by a tetrahedral structure in which the phosphorus atom is tetracoordinated. TSb3 lies 8.8 kcal/mol above INTb3. Unlike TSa2 in the A Pathway, both the p-orbital of the carbon from the methoxy group and the p-orbital of the oxygen O_2 from the sarin participate in the interactions with fluorine. The relative Gibbs free energy difference and equilibrium constant for this step are evaluated to be 6.8 kcal/mol and 1.0×10^{-5}, respectively, suggesting a little faster process of fluorine removal than the corresponding step in the A Pathway.

TSb3 is predicted to quickly form the intermediate INTb4. INTb4 is calculated to be 21.6 kcal/mol more stable than TSb3 (10.7 kcal/mol below the separated reactants), implying that INTb4 is stable and might be detected through experiments. A strong F−H···O hydrogen bond is found in INTb4 between the O_2 oxygen of the sarin−serine complex and the H_1 proton of the leaving HF, where the hydrogen bond distance is calculated to be 1.63 Å and the BCP density is estimated to be 0.0483 au. However, the energy of the separated products (sarin−serine adduct and HF) is 16.0 kcal/mol higher than that of the INTb4 intermediate. INTb4 is therefore expected to be the favorable stabilized product form in the B Pathway.

Although there are three steps in the B Pathway, the reactions of the second and third steps are fast and can be treated as a combined elimination process of fluorine. The above mechanism suggests that the first step (addition reaction) is the rate-determining step for the B Pathway, similar to the process predicted for the A Pathway.

With the inclusion of solvent effects using the PCM models, the PCM potential energy surface of the B Pathway (Figure 4) reveals almost the same characteristics as the gas-phase pathway. The differences between the energy barriers in gas phase and in solvent (water) are less than 2.4 kcal/mol. It can be concluded that the solvent has hardly any influence on the B Pathway.

Comparing the two pathways (A and B), both include a two step addition−elimination mechanism, and the first nucleophilic attack step (addition process) is the rate-determining step. However, the A Pathway is much easier to achieve than the B Pathway in the rate-determining step (about 10^7 faster). As for the elimination step (the removal of fluorine), the energy barriers for both pathways are similar. This suggests that the catalytic triad catalyzes the phosphonylation reaction of sarin and serine by speeding up the rate-determining step. The solvent plays a more important role in the A Pathway than in the B Pathway. The polar solvent helps to lower the activation energy and accelerates the entire phosphonylation reaction.

It is expected that the real biological phosphonylation reaction of sarin with AChE has characteristics that are between the parameters of the A Pathway and the B Pathway and that the energy barriers in such a case are lower than those of the B Pathway but higher than those of the A Pathway.

Conclusions

The potential energy surfaces for the models characterizing the phosphonylation of sarin and acetylcholinesterase have been theoretically studied at the B3LYP/6-311G(d,p) level of theory. Reactions under two different conditions, which represent the situation with and without the effect of the catalytic triad of AChE, respectively, have been probed (the A Pathway and the B Pathway). Stable trigonal bipyramidal intermediates are formed in both pathways. Moreover, the mechanisms of both pathways are consistent and suggest that the phosphonylation of the AChE active site is a two-step addition−elimination reaction, different from the previously proposed in-line replacement mechanism.[9,27−30] The first step (addition process) is the rate-determining step, while the ensuing steps are very rapid by comparison. The differences between the two pathways suggest that the catalytic triad of AChE is involved in the reaction by speeding up the phosphonylation process as it does in the acylation reaction between ACh and AChE.

The effect of aqueous solvation was accounted for via the polarizable continuum model (PCM) at the B3LYP/6-311G(d,p) level. The polar solvent (water) has negligible effects on the B Pathway. However, it lowers the activation energy and accelerates the entire phosphonylation reaction in the A Pathway. This suggests that the enzymatic reaction is influenced strongly by the solvent environment. It may be expected that, under real biological conditions, the phosphonylation of the AChE active site by sarin can occur easily.

As one of the referees suggested, the proposed steps of the reactions could be quickly verified spectroscopically through Stopped Flow.

Acknowledgment. This work was supported by a CMCM grant (2T34GM007672-25A1) and by the Army High Performance Computing Research Center under the auspices of the Department of the Army, Army Research Laboratory cooperative agreement number DAAD19-01-2-0014, the content of which does not necessarily reflect the position or the policy of the government, and no official endorsement should be inferred.

References and Notes

(1) Rosenberry, T. L. *Advances in Enzymology*; Meister, A., Ed.; Jon Wiley & Sons: New York, 1975; Vol. 43, pp 103−218.
(2) Quinn, D. M. *Chem. Rev.* **1987**, *87*, 955−975.
(3) Sussman, J. L.; Harel, M.; Frolow, F.; Oefner, C.; Goldman, A.; Toker, L.; Silman, I. *Science* **1991**, *253*, 872.
(4) Taylor, P.; Lappi, S. *Biochemistry* **1975**, *14*, 1989−1997.
(5) Harel, M.; Schalk, I.; Ehret-Sabatier, L.; Bouet, F.; Goeldner, M.; Hirth, C.; Axelsen, P. H.; Silman, I.; Sussman, J. L. *Proc. Natl. Acad. Sci. U.S.A.* **1993**, *90*, 9031−9035.
(6) Barak, D.; Ordentlich, A.; Kaplan, D.; Barak, R.; Mizrahi, D.; Kronman, C.; Segall, Y.; Velan, B.; Shafferman, A. *Biochemistry* **2000**, *39*, 1156−1161.
(7) Millard, C. B.; Koellner, G.; Ordentlich, A.; Shafferman, A.; Silman, I.; Sussman, J. L. *J. Am. Chem. Soc.* **1999**, *121*, 9883−9884.
(8) Millard, C. B.; Kryger, G.; Ordentlich, A.; Greenblatt, H. M.; Harel, M.; Raves, M. L.; Segall, Y.; Barak, D.; Shafferman, A.; Silman, I.; Sussman, J. L. *Biochemistry* **1999**, *38*, 7032−7039.
(9) Bencsura, A.; Enyedy, I. Y.; Kovach, I. M. *Biochemistry* **1995**, *34*, 8989−8999.
(10) Barak, D.; Kaplan, D.; Ordentlich, A.; Ariel, N.; Velan, B.; Shafferman, A. *Biochemistry* **2002**, *41*, 8245−8252.
(11) Wlodek, S. T.; Antosiewicz, J.; Briggs, J. M. *J. Am. Chem. Soc.* **1997**, *119*, 8159−8165.
(12) Fuxreiter, M.; Warshel, A. *J. Am. Chem. Soc.* **1998**, *120*, 183−194.
(13) Vagedes, P.; Rabenstein, B.; Åqvist, J.; Marelius, J.; Knapp, E. *J. Am. Chem. Soc.* **2000**, *122*, 12254−12262.
(14) Quinn, D. M.; Feaster, S. R.; Nair, H. K.; Baker, N. A.; Radić, Z.; Taylor, P. *J. Am. Chem. Soc.* **2000**, *122*, 2975−2980.
(15) Malany, S.; Sawai, M.; Sikorski, R. S.; Seravalli, J.; Quinn, D. M.; Radić, Z.; Taylor, P.; Kronman, C.; Velan, B.; Shafferman, A. *J. Am. Chem. Soc.* **2000**, *122*, 2981−2987.
(16) Nachon, F.; Asojo, O. A.; Borgstahl, G. E. O.; Masson, P.; Lockridge, O. *Biochemistry* **2005**, *44*, 1154−1162.
(17) Berkman, C. E.; Ryu, S.; Quinn, D. A.; Thompson, C. M. *Chem. Res. Toxicol.* **1993**, *6*, 28−32.
(18) Tougu, V. *Curr. Med. Chem. − Central Nervous System Agents* **2001**, *1*, 155−170.
(19) Hovanec, J. W.; Lieske, C. N. *Biochemistry* **1972**, *11*, 1051−1056.
(20) Saxena, A.; Maxwell, D. M.; Quinn, D. M.; Radić, Z.; Taylor, P.; Doctor, B. P. *Biochem. Pharmacol.* **1997**, *54*, 269−274.
(21) Maxwell, D. M.; Brecht, K. M. *Chem. Res. Toxicol.* **1992**, *5*, 66−71.

(22) Wang, J.; Roszak, S.; Gu, J.; Leszczynski, J. *J. Phys. Chem. B* **2005**, *109*, 1006−1014.

(23) Ordentlich, A.; Barak, D.; Kronman, C.; Benschop, H. P.; De Jong, L. P. A.; Ariel, N.; Barak, R.; Segall, Y.; Velan, B.; Shafferman, A. *Biochemistry* **1999**, *38*, 3055−3066.

(24) Elhanany, E.; Ordentlich, A.; Dgany, O.; Kaplan, D.; Segall, Y.; Barak, R.; Velan, B.; Shafferman, A. *Chem. Res. Toxicol*. **2001**, *14*, 912−918.

(25) Bencsura, A.; Enyedy, I. Y.; Kovach, I. M. *J. Am. Chem. Soc*. **1996**, *118*, 8531−8541.

(26) Bennet, A. J.; Kovach, I. M.; Schowen, R. L. *J. Am. Chem. Soc*. **1988**, *110*, 7892−7893.

(27) George, K. M.; Schule, T.; Sandoval, L. E.; Jennings, L. L.; Taylor, P.; Thompson, C. M. *J. Biol. Chem.* **2003**, *278*, 45512−45518.

(28) Enyedy, I.; Bencsura, A.; Kovach, I. M. *Phosphorus, Sulfur Silicon* **1996**, 109−110.

(29) Sterri, S. H.; Fonnum, F. *Biochem. Pharmacol*. **1987**, *36*, 3937−3942.

(30) Kovach, I. M. *J. Enzyme Inhib*. **1988**, *2*, 199−208.

(31) Thompson, C. M.; Ryu, S.; Berkman, C. E. *J. Am. Chem. Soc*. **1992**, *114*, 10710−10715.

(32) Kovarik, Z.; Radić, Z.; Berman, H. A.; Simeon-Rodelf, V.; Reiner, E.; Taylor, P. *Biochemistry* **2004**, *43*, 3222−3229.

(33) Kovach, I. M.; Huber, J. H.; Schowen, R. L. *J. Am. Chem. Soc*. **1988**, *110*, 590−593.

(34) Šečkutė, J.; Menke, J. L.; Emnett, R. J.; Patterson, E. V.; Cramer, C. J. *J. Org. Chem.* **2005**, *70*, 8649−8660.

(35) Becke, A. D. *J. Chem. Phys*. **1993**, *98*, 5648−5652.

(36) Lee, C.; Yang, W.; Parr, R. G. *Phys. Rev. B* **1988**, *37*, 785−789.

(37) Miehlich, B.; Savin, A.; Stoll, H.; Preuss, H. *Chem. Phys. Lett*. **1989**, *157*, 200−206.

(38) Hehre, W. J.; Radom, L.; Schleyer, P. R.; Pople, J. A. *Ab Initio Molecular Orbital Theory*; Wiley: New York, 1986.

(39) Reed, A. E.; Weinstock, R. B.; Weinhold, F. *J. Chem. Phys*. **1985**, *83*, 735.

(40) Reed, A. E.; Weinhold, F. *J. Chem. Phys*. **1985**, *83*, 1736.

(41) Reed, A. E.; Curtiss, L. A.; Weinhold, F. *Chem. Rev*. **1988**, *88*, 899.

(42) Reed, A. E.; Schleyer, P. R. *J. Am. Chem. Soc*. **1990**, *112*, 1434.

(43) Frisch, M. J.; Trucks, G. W.; Schlegel, H. B.; Scuseria, G. E.; Robb, M. A.; Cheeseman, J. R.; Montgomery, J. A., Jr.; Vreven, T.; Kudin, K. N.; Burant, J. C.; Millam, J. M.; Iyengar, S. S.; Tomasi, J.; Barone, V.; Mennucci, B.; Cossi, M.; Scalmani, G.; Rega, N.; Petersson, G. A.; Nakatsuji, H.; Hada, M.; Ehara, M.; Toyota, K.; Fukuda, R.; Hasegawa, J.; Ishida, M.; Nakajima, T.; Honda, Y.; Kitao, O.; Nakai, H.; Klene, M.; Li, X.; Knox, J. E.; Hratchian, H. P.; Cross, J. B.; Bakken, V.; Adamo, C.; Jaramillo, J.; Gomperts, R.; Stratmann, R. E.; Yazyev, O.; Austin, A. J.; Cammi, R.; Pomelli, C.; Ochterski, J. W.; Ayala, P. Y.; Morokuma, K.; Voth, G. A.; Salvador, P.; Dannenberg, J. J.; Zakrzewski, V. G.; Dapprich, S.; Daniels, A. D.; Strain, M. C.; Farkas, O.; Malick, D. K.; Rabuck, A. D.; Raghavachari, K.; Foresman, J. B.; Ortiz, J. V.; Cui, Q.; Baboul, A. G.; Clifford, S.; Cioslowski, J.; Stefanov, B. B.; Liu, G.; Liashenko, A.; Piskorz, P.; Komaromi, I.; Martin, R. L.; Fox, D. J.; Keith, T.; Al-Laham, M. A.; Peng, C. Y.; Nanayakkara, A.; Challacombe, M.; Gill, P. M. W.; Johnson, B.; Chen, W.; Wong, M. W.; Gonzalez, C.; Pople, J. A. *Gaussian 03*, revision C.02; Gaussian, Inc.: Pittsburgh, PA, 2003.

(44) Bader, R. F. W. *Atoms in Molecules: a Quantum Theory*; Clarendon Press: Oxford, 1990.

(45) Bader, R. F. W. *Chem. Rev*. **1991**, *91*, 893.

(46) Biegler-König, F.; Schönbohm, J.; Bayles, D. *J. Comput. Chem.* **2001**, *22*, 545−559.

(47) Cossi, M.; Barone, V.; Cammi, R.; Tomasi, J. *Chem. Phys. Lett*. **1996**, *255*, 327−335.